Department of Pharmacology[1], Institute of Medical Sciences, Shanghai Jiao Tong University School of Medicine,; Department of Pharmaceutics[2], Key Laboratory of Smart Drug Delivery, Ministry of Education & PLA, School of Pharmacy, Fudan University, Shanghai, PR China

High-density lipoprotein-biomimetic nanocarriers for glioblastoma-targeting delivery: the effect of shape

Jia-Lin Huang[1], Gan Jiang[1], Qing-Xiang Song[1], Xiao Gu[1], Hua-Hua Song[1], Xiao-Lin Wang[1], Di Jiang[2], Ting Kang[2], Xing-Ye Feng[2], Xin-Guo Jiang[2], Hong-Zhuan Chen[1], Xiao-Ling Gao[1]

Received May 20, 2016, accepted July 29, 2016

Xiao-Ling Gao and Hong-Zhuan Chen, Department of Pharmacology, Institute of Medical Sciences, Shanghai Jiao Tong University School of Medicine, 280 South Chongqing Road, Shanghai, 200025, PR China
shellygao1@sjtu.edu.cn
hongzhuan_chen@hotmail.com

Pharmazie 71: 709–714 (2016) *doi: 10.1691/ph.2016.6081*

Rational design of the physicochemical properties of nanocarriers can optimize their pharmacokinetics, bio-distribution, intratumoral penetration and tumor bioavailability. In particular, particle shape is one of the crucial parameters that can impact the circulation time, tumor accumulation and tumor cell internalization of nanocarrier. Biomimetic reconstituted high-density lipoprotein (rHDL), by mimicking the endogenous shape and structure of high-density lipoprotein, has been indicated as a promising tumor-targeting nanoparticulate drug delivery system whereas the effect of shape on tumor-targeting efficiency has not been fully evaluated. Herein, we constructed apolipoprotein E-based biomimetic rHDL in both discoidal form (d-rHDL) and spherical form (s-rHDL), and compared their efficiency in glioblastoma multiforme (GBM)-targeting delivery. s-rHDL showed higher cellular association in GBM cells especially at a high exposure dosage or after a long incubation time. Moreover, it exhibited deeper penetration in 3D GBM spheroids *in vitro* and higher accumulation at the GBM site *in vivo* with the GBM-targeting accumulation of s-rHDL increased by 73% when compared with that of d-rHDL at 24 h post-injection. The findings collectively indicated that s-rHDL might serve as a more efficient nanocarrier for glioblastoma-targeting drug delivery.

1. Introduction

Glioblastoma multiforme (GBM), the most lethal brain tumor in both children and adults, is still of poor prognosis despite the comprehensive treatments comprising surgical resection and chemo/radiation therapy (Siegel et al. 2013; Grossman et al. 2010). Although systemic chemotherapy plays a crucial role in clinical practice, the efficiency is still far from satisfaction due to the drug delivery problem, which is majorly ascribed to the existence of blood–brain barrier (BBB) and blood–brain tumor barrier (BBTB) (Hendricks et al. 2015; Oberoi et al. 2016).

The development of nanoparticulate drug delivery systems are making a significant contribution to the improvement of drug delivery in cancer and many of these technologies can be applied to anti-GBM drug delivery. The requirements for an ideal tumor-targeting delivery system include the following: efficient accumulation in the tumor, efficient penetration/diffusion within tumor regions, and efficient intracellular delivery. Biomimetic reconstituted high-density lipoprotein (rHDL), by mimicking the endogenous shape and structure of high-density lipoprotein (HDL), is a promising tumor-targeting delivery system that may meet these requirements (Kuai et al. 2016). Firstly, rHDL can remain in circulation for an extended period of time (circulating half-life 12–24 h), allowing accumulation of rHDL in tumor regions by the enhanced permeability and retention (EPR) effect. Secondly, as the openings in the extracellular matrix of tumor cells are generally less than 40 nm (Ng et al. 2011), rHDL nanoparticles which are typically within a diameter range of 10-20 nm, would penetrate and diffuse efficiently throughout tumor regions. And thirdly, as cancer cells often require cholesterol and other membrane components for rapid proliferation, the unique feature of transporting cholesterol, phospholipids, triglycerides, proteins, and vitamins made rHDL a promising nanocarrier to deliver cargo into specific tumor cells more efficiently (Li et al. 2006; Salloum et al. 2014; Foster 2013; Das 2011). Actually, rHDL containing recombinant apolipoprotein A proteins or apolipoprotein A mimetic peptides has been reported to efficiently deliver therapeutic agents to various types of cancer cells (Lin et al. 2012; Mooberry et al. 2010; Cho 2009). In the case of GBM-targeting drug delivery, due to the relatively high expression of the receptors of apolipoprotein E (ApoE) on the BBB, BBTB and GBM cells, we proposed that ApoE-based rHDL might represent an efficient GBM-targeting nanocarrier (Croy et al. 2004; Prevost and Raussens 2004; Zhang et al. 2013).

Naturally occurring high-density lipoprotein (HDL) exists in two distinct structures as discoidal and spherical forms during the metabolic process. Cholesterol ester can be incorporated into the core of native HDL particle, initiating the transformation from discoidal form to spherical form, which is induced by the activation of lecithin cholesterol acyltransferase (LCAT) (Liang et al. 1996; Rader 2006). The ability to transport lipid, proteins and microRNAs to recipient cells suggested that both discoidal and spherical HDL play crucial roles in the intercellular communication (Vickers et al. 2011), whereas the performances and metabolic fates of discoidal and spherical HDL are well known to be quite different *in vivo* (Zhang et al. 2013). For the development of rHDL-based nanomedicine, the change of lipid composition would largely affect the shape of rHDL. Rational design of the physicochemical properties of nanocarriers, including size, shape, surface charge and surface chemistry, can optimize their pharmacokinetics, bio-distribution, intratumoral penetration and tumor bioavailability. In particular, particle shape has been demonstrated as one of the most crucial parameters that impact the circulation time, tumor accumulation and tumor cell internalization efficiency of polymersomes-based nanocarrier (Wang et al. 2014; Ernsting et al. 2013). It's very possible that shape might also affect the biofate of rHDL. In addition, previous reports demonstrated that a minor increase in thera-

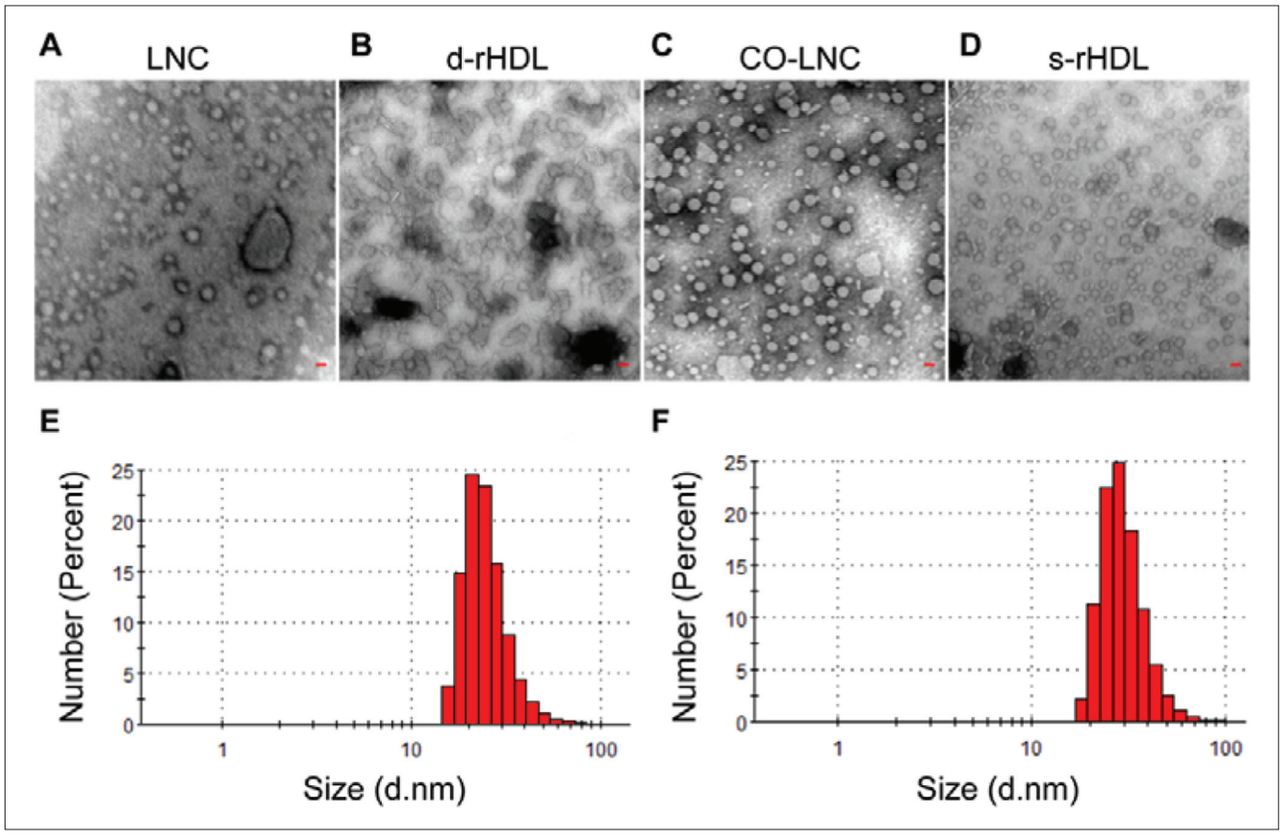

Fig. 1: Characterization of d-rHDL and s-rHDL. Morphology and particle size of LNC (A), d-rHDL (B), CO-LNC (C) and s-rHDL (D) under a transmission electron microscope after negative staining with sodium phosphotungstate solution (1.75%, w/v). Scale bar, 20 nm. Particle size distribution of d-rHDL (E) and s-rHDL (F) analyzed by dynamic light scattering via a Zetasizer.

peutic diffusion rates or nanoparticle distribution is sufficient to profoundly improve the therapeutic effectiveness (Diop-Frimpong et al. 2011; Tong et al. 2004; Jain et al. 2006). As both discoidal and spherical rHDL can be used for drug loading without change the shape of the carrier (Huang et al. 2015; Wang et al. 2013; McConathy et al. 2008), therefore, a meaningful comparison of the spherical form versus discoidal form of rHDL in drug delivery efficiency may serve as a guideline in engineering artificial rHDL nanocarrier for GBM-targeting delivery.

In order to study the effect of shape of rHDL for GBM-targeting delivery, in the current study, we prepared discoidal rHDL (d-rHDL) composing of DMPC and ApoE and spherical rHDL (s-rHDL) composing of cholesteryl oleate (CO), DMPC and ApoE, to mimic the different stage of natural HDL, and determined their accumulation and penetration at the GBM site and cellular internalization into GBM cells both *in vitro* and *in vivo*. According to our previously work (Song et al. 2014), a film hydration method was used for the preparation of the biomimetic nanoparticles. Transmission electron microscopy (TEM) was used to characterize the shape of d-rHDL and s-rHDL. The uptake efficiency of d-rHDL and s-rHDL was qualitatively and quantitively evaluated in C6 glioblastoma cells. The shape-dependent penetration ability of rHDL was determined by using C6 3D tumor spheroids *in vitro*, and in C6 tumor-bearing nude mice *in vivo via* real-time fluorescent imaging in mice model and *in situ* distribution analysis in frozen brain slides.

2. Investigations, results and discussion

2.1. Characterization of d-rHDL and s-rHDL

Dynamic Light Scattering (DLS) analysis showed that the size of d-rHDL was 26.93±2.60 nm. After encapsulating CO as the cores, the size slightly increased to 30 nm with the same narrow size distribution. Both nanocarriers (≤50 nm) can take advantage of the small size to penetrate BBB and transport into the poorly permeable GBM parenchyma (Cabral et al. 2011; Lee et al. 2010). In contrast, in the absence of ApoE, the particle sizes of LNC and CO-LNC, the relevant control nanoparticles of d-rHDL and s-rHDL, were both above 30 nm with a bigger polydispersity index. The zeta potential of d-rHDL was -6.39±0.45 mV, while that of s-rHDL was -11.47±1.24 mV, both more negative than their control nanoparticles (LNC and CO-LNC), indicating that negative-charged ApoE3 had been anchored on the surface of lipid membrane (Zhang et al. 2011; Gessner et al. 2002). Such a zeta potential of about -10 mV is typical for neutral nanoparticles (within ±10 mV) exhibiting the least mononuclear phagocyte system interaction and the longest circulation (Li and Huang 2008; Levchenko et al. 2002). In addition, from the Table , we can see that fluorescent labeling did not change either the size or the zeta potential of both d-rHDL and s-rHDL. Under TEM, d-rHDL exhibited a distinct multilayer discoidal morphology, while s-rHDL exhibited a spherical morphology, which suggested that the constructed d-rHDL and s-rHDL may mimic both forms of HDL (Fig. 1).

Table: Particle size and zeta potential of the nanocarriers

	Particle size (nm)	Polydispersity index	Zeta potential (mV)
LNC	30.95±1.59	0.36	-4.50±1.31
d-rHDL	26.93±2.60	0.27	-6.39±0.45
CO-LNC	32.24±1.07	0.39	-7.4±0.61
s-rHDL	30.57±5.51	0.25	-11.47±1.24
DiI-labeled d-rHDL	24.62±1.59	0.35	7.29±0.56
DiI-labeled s-rHDL	34.47±5.51	0.30	13.83±2.48
DiR-labeled d-rHDL	25.66±5.15	0.31	4.43±1.43
DiR-labeled s-rHDL	33.79±3.90	0.34	-11.70±1.42

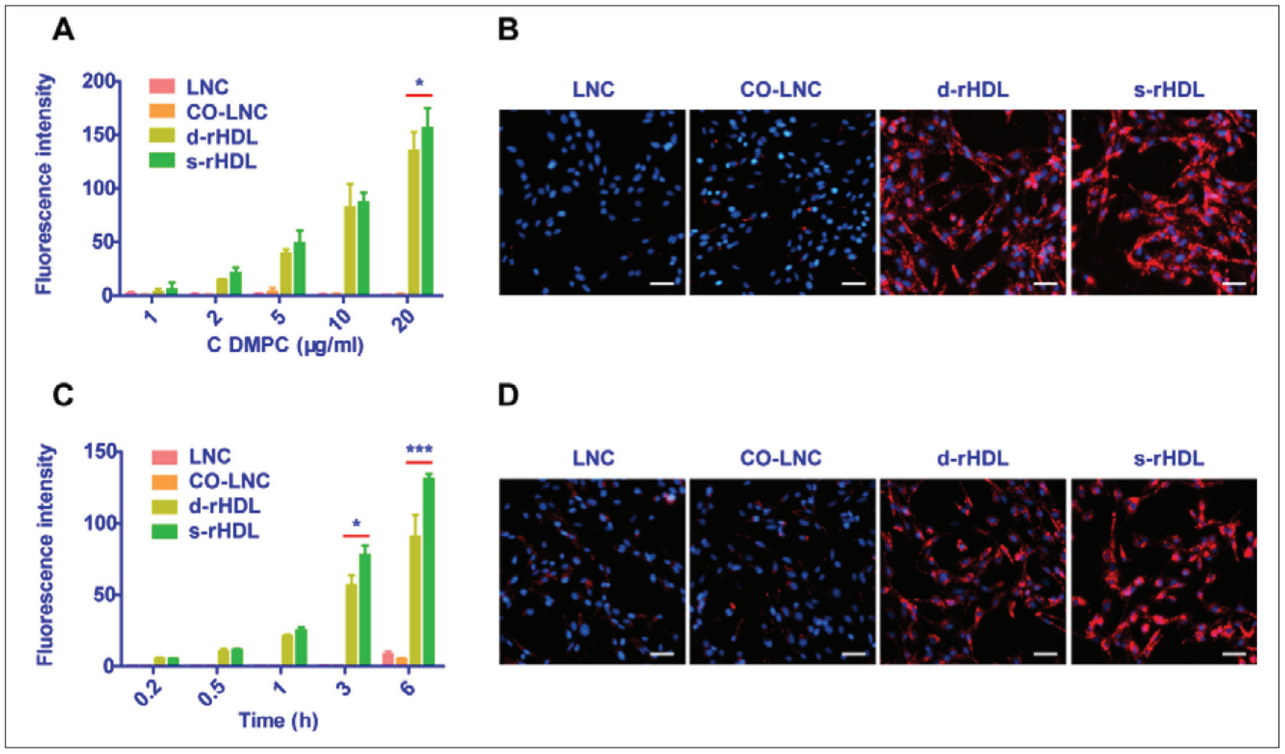

Fig. 2: Shape-dependent efficiency of cellular uptake of d-rHDL and s-rHDL in glioblastoma cells. (A) Quantitative cellular uptake of DiI-labeled LNC, CO-LNC, d-rHDL and s-rHDL in C6 glioblastoma cells at 37 °C, respectively, after incubation for 3 h at the DMPC concentrations from 1 mg/mL to 20 mg/mL. (B) Qualitative observation of the cellular uptake of DiI-labeled LNC, CO-LNC, d-rHDL and s-rHDL after incubation for 3 h at the DMPC concentration of 20 mg/mL in C6 glioblastoma cells at 37 °C. Red: DiI-labeled nanoparticles. Blue: nuclei. Scale bar, 50 mm. (C) Quantitative cellular uptake of DiI-labeled LNC, CO-LNC, d-rHDL and s-rHDL in C6 glioblastoma cells after different incubation time ranged from 0.2 to 6 h at the DMPC concentration of 5 mg/mL at 37 °C. (D) Qualitative observation of the cellular uptake of DiI-labeled LNC, CO-LNC, d-rHDL and s-rHDL after incubation for 6 h at the DMPC concentration of 5 mg/mL in C6 glioblastoma cells at 37°C. Red: DiI-labeled nanoparticles. Blue: nuclei. Scale bar, 50 mm. For A and C, data represented mean ± s.d. (n=3). *p<0.05 and ***p<0.001 significantly higher than the cellular uptake of d-rHDL at 37 °C. The significance of the differences was evaluated by Student's t-test.

2.2. *Shape-dependent uptake efficiency of d-rHDL and s-rHDL in glioblastoma cells*

Efficient cellular uptake is the basic requirement for glioblastoma drug delivery strategy. The cellular uptake of d-rHDL and s-rHDL in a C6 glioblastoma cell line was evaluated quantitatively under a Kinetic Scan HCS Reader. We added DiI in the lipid film to serve as the fluorescent probe. As shown in Fig. 2A and 2C, the cellular uptake of d-rHDL and s-rHDL was both concentration and incubation time dependent. After 3-h incubation, the cellular uptake of s-rHDL was slightly higher but not significantly different with that of d-rHDL at the DMPC concentration ranged from 1 to 10 mg/mL but increased by 16% at the concentration of 20 mg/mL (*p<0.05). At a relatively low concentration (5 mg/mL), after 6-h incubation, the cellular uptake of s-rHDL increased by 40% when compared with that of d-rHDL (***p<0.001). Similarly, qualitative analysis through fluorescent microscopy analysis showed that the cellular internalized fluorescence intensity of s-rHDL was higher than that of d-rHDL at the concentration of 20 mg/mL after 3-h incubation (Fig. 2B). As shown in Fig. 2D, the superiority of s-rHDL nanocarrier became more obvious after a longer incubation time (eg. 6 h). The interesting phenomena collectively indicated that s-rHDL can be internalized into the GBM cells more efficiently *in vitro*, especially at a high exposure dosage or after a long incubation time. And such phenomenon could be caused by the following reasons. Firstly, from the TEM images (Fig. 1B and 1D), it can be found that the dispersity of s-rHDL was more uniform than that of d-rHDL especially at higher concentrations, which may result in a higher extent of interaction between s-rHDL and cellular surface and lead to a higher cellular uptake. In addition, s-rHDL which containing CO could be more favored by the cancer cells lacking of nutrient. Moreover, the cellular associated fluorescence intensity of d-rHDL and s-rHDL were both significantly higher than that of LNC and CO-LNC at all incubation concentrations and time points. The phenomena suggested that the incorporation of ApoE into LNC and CO-LNC played an important role in facilitating the cellular uptake of the nanocarriers.

2.3. *Shape-dependent penetration of d-rHDL and s-rHDL in 3D glioblastoma spheroids*

Considering the superior uptake efficiency of s-rHDL in C6 cells, we examined if s-rHDL could penetrate into 3D glioblastoma spheroids more effectively than d-rHDL. 3D glioblastoma spheroids, which can mimic the physiologic barriers in solid tumors (heterogeneous tumor perfusion, high cell density, acidic PH and increased interstitial pressure), were cultured and subjected to confocal microscopy analysis following the incubation with DiI-labeled LNC, CO-LNC, d-rHDL and s-rHDL for 3 h at the DMPC concentration of 100 mg/mL (Hirschhaeuser et al. 2010). It was found that s-rHDL penetrated deep and distributed extensive in the C6 3D glioblastoma spheroids. In contrast, a lower level of fluorescent intensity of d-rHDL was found associated with the spheroids (Fig. 3). Quantitative analysis showed that the penetration depth of s-rHDL was 100 mm while that of d-rHDL was only 75 mm. These findings provided the evidence that s-rHDL could access the inside of the solid tumors more efficiently and enhance the cellular uptake by those cancer cells that located at the 'blind areas' more powerfully (Chauhan et al. 2011). Predictably, the poor cellular uptake ability resulted in poor fluorescent intensity of LNC and CO-LNC in 3D glioblastoma spheroids.

2.4. *In vivo glioblastoma-targeting distribution of biomimetic nanocarrier and its shape dependence*

To demonstrate the efficiency of tumor-targeting delivery of s-rHDL and d-rHDL *in vivo*, we performed real-time fluorescent imaging and *in situ* distribution analysis in frozen brain slides with

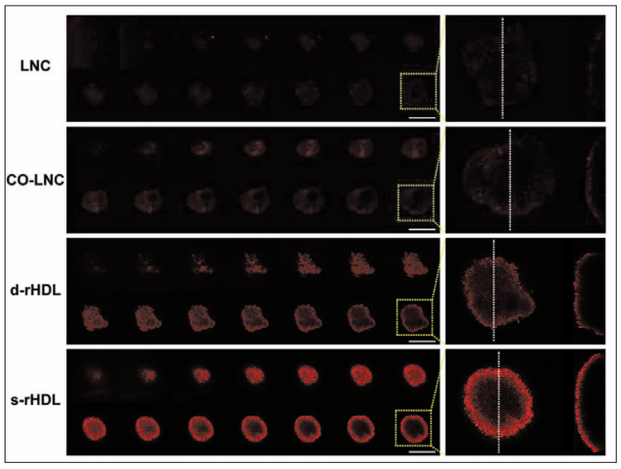

Fig. 3: Confocal microscopy analysis of the penetration of DiI-labeled LNC, CO-LNC, d-rHDL and s-rHDL in avascular C6 3D tumor spheroids. Multi-level scan of the penetration of DiI-labeled LNC, CO-LNC, d-rHDL and s-rHDL started at the top of the spheroid and the interval between the consecutive slides was 5 mm. Scale bar, 500 mm.

the orthotopic transplantation GBM mouse model. As shown in Fig. 4A, compared with d-rHDL, s-rHDL exhibited a constant superiority in GBM targeting with higher fluorescent intensity at the tumor site at each time point after-injection. This was further confirmed by the semi-quantitative analysis of fluorescent intensity which showed that the fluorescent intensity of s-rHDL in the glioblastoma region was 0.51, 0.7, 0.92 and 1.3-fold higher than that of d-rHDL at 4 h, 8 h, 12 h and 24 h post-injection, respectively (Fig. 4C). Similar results were obtained by the analysis of the accumulation of the nanostructures in the isolated organs at 24 h post-injection, in which a significant higher fluorescent intensity of s-rHDL was found in the GBM site (Fig. 4B) with the fluorescent intensity of s-rHDL increased by 73% when compared with that of d-rHDL. The frozen tumor sections were observed under a laser scanning confocal microscopy at 3 h post-injection. It was found that in the tumor region the accumulation of s-rHDL and d-rHDL were much higher than that in the adjacent normal brain site (Fig. 5), which may be contributed by the receptor-mediated internalization and EPR effect (Fang et al. 2011). Simultaneously, lower accumulations of LNC and CO-LNC were observed in tumor sites, confirming that ApoE3-reconstituted lipoprotein could overcome BBB, BBTB and enormously accumulated at the glioma site. In particular, s-rHDL showed much higher tumor-specific accumulation which was in great accordance with the real-time fluorescent imaging results.

Compared with the cellular uptake data *in vitro*, the *in vivo* analysis found more obvious superiority in GBM-targeting accumulation and penetration achieved by s-rHDL over d-rHDL especially at a longer circulation time. Beside the higher dispersity of s-HDL and its loading with the nutrient CO that may be more favored by cancer cells, the different metabolic process between s-rHDL and d-rHDL *in vivo* could be another key point that resulted in the superiority of s-rHDL in *in vivo* GBM-targeting drug delivery. The biological interaction between d-rHDL and LCAT might cause the instability of the nanostructure especially after a long circulation time and thus lower its accumulation in the tumor region. In contrast, as the bulk of plasma lipoproteins, lipid-enriched s-HDL is more similar to mature HDL counterparts and exhibits less tendency to interact with LCAT, which would thus achieve higher tumor-targeting efficiency.

2.5. Conclusion

In the present work, we formulated and characterized both discoidal and spherical rHDL for GBM-targeting delivery. Both nanocarriers were found to be internalized efficiently into the C6 glioblastoma cells and 3D tumor spheroids *in vitro*, and distributed deeply into the glioblastoma region *in vivo*. Specifically, compared with d-rHDL, s-rHDL was internalized to a greater extent and exhibited higher GBM-targeting efficiency, which could be contributed by the higher dispersity, loading with nutrient and higher metabolic stability of s-rHDL. Collectively, we demonstrated that s-rHDL may be more effective for GBM-targeting delivery and the findings of this study may provide important information for the design of HDL-mimetic nanocarriers for glioblastoma-targeting drug delivery.

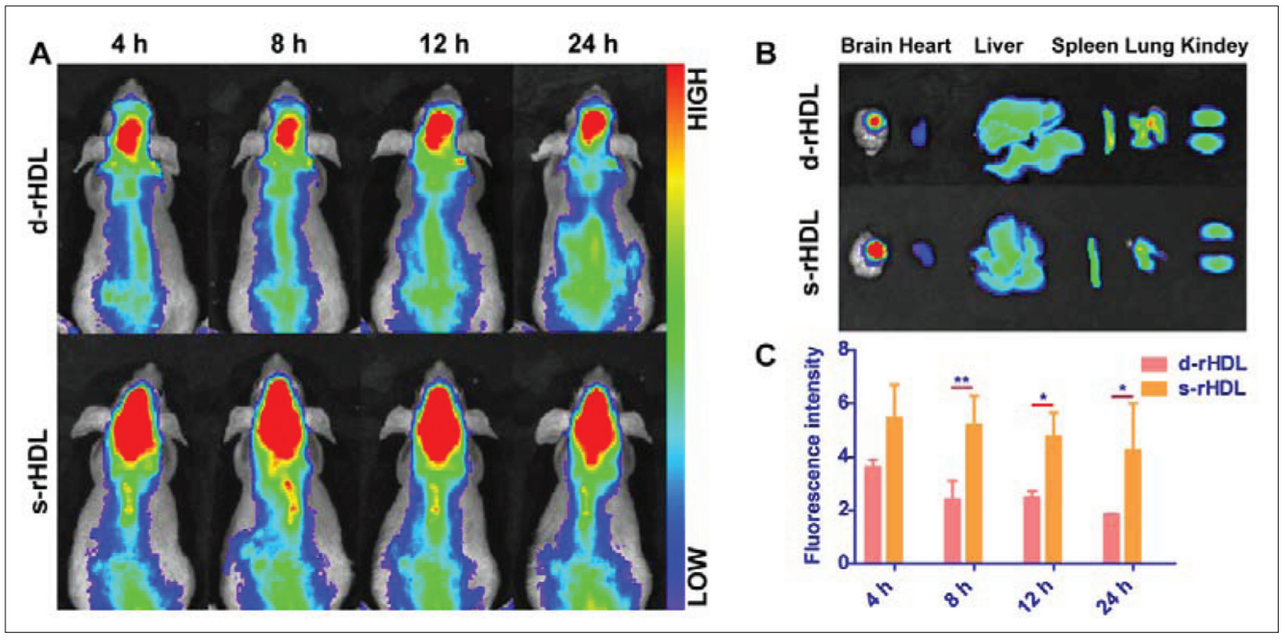

Fig. 4: *In vivo* glioblastoma-targeting efficiency of biomimetic rHDL and its shape-dependent biodistribution. (A) *In vivo* real-time fluorescent imaging of mice bearing intracranial C6 glioblastoma at 4, 8, 12 and 24 h after intravenously injected with DiR-labeled d-rHDL and s-rHDL. (B) Distribution of the fluorescent signals of DiR-labeled d-rHDL and s-rHDL in various organs at 24 h post-injection. (C) Semi-quantitative analysis of the fluorescent intensity of DiR-labeled d-rHDL and s-rHDL in glioblastoma regions at 4, 8, 12 and 24 h post-injection. Data represented mean ± s.d. (n=3). *p<0.05 and **p<0.01 significantly different with that of d-rHDL.

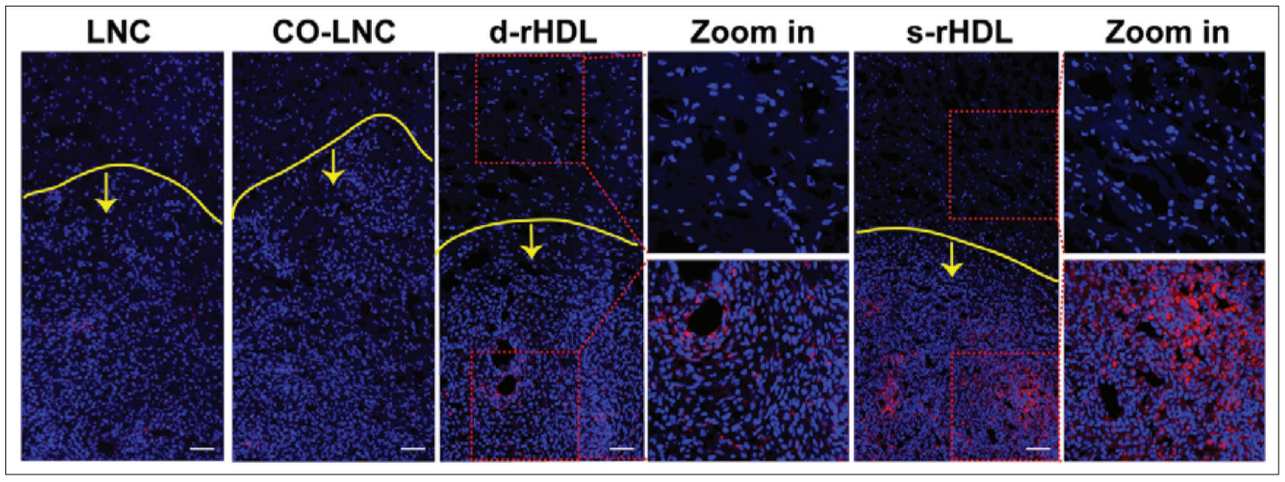

Fig. 5: Brain distribution of DiI-labeled LNC, CO-LNC, d-rHDL and s-rHDL at 3 h post-injection. Yellow lines showed the boundary between glioblastoma and normal brain tissue. Arrows indicated the glioblastoma zones. Scare bar: 100 mm.

3. Experimental

3.1. Materials

1,2-Dimyristoyl-sn-glycero-3-phosphocholine (DMPC) was obtained from Avanti Polar Lipids, Inc. (Alabaster, AL, USA). Full-length ApoE3 was provided by PEPROTECH, Inc. (Rocky Hill, NJ, USA). 1,1'-dioctadecyl-3,3,3',3'-tetramethylindocarbocyanine perchlorate (DiI) was purchased from Invitrogen, Inc. (Carlsbad, CA, USA). 1,1'-dioctadecyl-3,3,3',3'-tetramethylindotricarbocyanine iodide (DiR), Hoechst 33258 and cholesteryl oleate (CO) were provided by Sigma-Aldrich, Inc. (St. Louis, MO, USA). 4,6-Diamidino-2-phenylindole (DAPI) was purchased from Molecular Probes, Inc. (Eugene, OR, USA). Other chemicals were obtained from Sigma-Aldrich unless otherwise indicated. All cell culture reagents were purchased from Gibco, Inc. (Grand Island, NY, USA) unless otherwise indicated.

3.2. Cells

Rat C6 glioblastoma cells were obtained from Cell Institute of Chinese Academy of Sciences (Shanghai, China) and cultured at 37 °C in an atmosphere of 5% CO_2 using the culture medium containing DMEM, 10% FBS, 1% L-glutamine, 1% penicillin-streptomycin solution and 1% nonessential amino acids.

3.3. Animals

Balb/c nude mice (male, 4-5 weeks, 20±2 g) were purchased from the Shanghai SLAC Laboratory Animal CO. LTD (Shanghai, China). The animals were housed in the specific pathogen-free animal facility with free access to food and water. All animal experiments were approved by the Animal Experimentation Ethics Committee of approved by the appropriate ethical committee of Shanghai Jiao Tong University School of Medicine.
In order to establish C6 tumor-bearing nude mice model, the suspension of C6 cells (500,000 cells/5 mL in pH 7.4 PBS) were injected into right corpus striatum of nude mice with the help of a stereotactic apparatus. These mice were allowed to recover for two weeks and used for subsequent experiments.

3.4. Preparation and characterization of d-rHDL and s-rHDL nanocomplex

Reconstituted high-density lipoprotein was prepared through the procedure previously described (Song et al. 2014). To prepare d-rHDL, 4 mg of DMPC, a neutral lipid, was dissolved in chloroform and the solution was dried under a high vacuum for 1 h at room temperature using a BüchiRotavapor R-200 (Büchi, Germany). The lipid film was then rehydrated in 4 mL of 0.01 mol/L PBS buffer (pH 7.4) by vortexing intermittently for 10 min. After brief sonication, the obtained lipid nanocarrier named LNC was then stored at 4 °C for further use. Finally, apoE3 (0.8 mg) was added into the above LNC solution (containing 4 mg DMPC) and incubated at 37 °C for 36 h. For the preparation of CO-LNC, 4 mg of DMPC and 124 mg CO was used for the formation of the lipid membrane, and the following preparation steps were similar with that for the preparation of LNC. Similarly, apoE3 (0.8 mg) was added into the above CO-LNC solution (containing 4 mg DMPC) and incubated at 37 °C for 36 h to prepare s-rHDL. DiI and DiR-labeled nanoparticles were prepared with the same procedure by adding DiI and DiR in the DMPC solution.
The morphology and size of LNC, d-rHDL, CO-LNC and s-rHDL were observed under a Hitachi H-7650 transmission electron microscope (Hitachi, Inc., Japan) after negative staining with 1.75% sodium phosphotungstate solution. The particle size distributions and zeta potential were measured by photon correlation spectroscopy (Zetasizer Nano-ZS90, Malvern Instruments, U.K.) utilizing a 4.0 mW He-Ne laser operating at 633 nm and a detector angle of 90°.

3.5. Quantification of cellular uptake of d-rHDL or s-rHDL

C6 cells were seeded into 96-well plates at the density of 5,000 cells/well and allowed to attach for 24 h. After that, the cells were exposed to a series concentration of DiI-labeled LNC, CO-LNC, d-rHDL or s-rHDL. For qualitative experiment, the nanoparticles were added at the DMPC concentration ranged from 1 to 20 mg/mL. After incubation at 37 °C for 3 h, the cells were washed twice with cold PBS buffer, fixed with 4% formaldehyde for 15 min, and then subjected to fluorescent microscopy analysis (Leica DMI4000 B, Germany) after staining with Hoechst 33258. For quantitative analysis, after fixation, the cells were nuclei-stained with Hoechst 33258 for 15 min away from light and then subjected to analysis under a Kinetic Scan HCS Reader (Thermo scientific, USA). For evaluating the time related cellular association of the nanoparticles, the incubation time was ranged from 0.2 to 6 h at the DMPC concentration of 5 μg/mL.

3.6. Penetration in tumor spheroids

For multicellular tumor spheroids formation, C6 cells were seeded in a 48-well plate pre-coated with 2% (w/v) agarose gel at the density of 2,000 cells/well. After cultured for 7 days, those uniform and compact spheroids were selected for further experiments. In order to study the penetration ability of the different nanocarriers, the spheroids were exposed to DiI-labeled LNC, CO-LNC, d-rHDL or s-rHDL at the DMPC concentration of 100 mg/mL. Three hours later, the tumor spheroids were washed with cold PBS for three times, fixed with 4% formaldehyde for 30 min and then subjected to laser scanning confocal microscopy analysis (LSM510, Leica, Germany).

3.7. In vivo real-time imaging and glioblastoma distribution

The bio-distribution of DiR-labeled d-rHDL and s-rHDL in C6 tumor-bearing nude mice following intravenous administration was studied *via* a Maestro *in vivo* imaging system (CRi, MA, USA) at the excitation wavelength 748 nm and emission wavelength 780 nm. Six mice were randomly divided into two groups and intravenously received DiR-labeled nanocarriers at the dose of DMPC 20 mg/kg. The fluorescent images were taken at the pre-determined time points (4, 8, 12, 24 h). Then the tumor-bearing mice were sacrificed at 24 h post-injection with the organs harvested for *ex vivo* imaging.
To evaluate the ability of LNC, CO-LNC, d-rHDL and s-rHDL in penetrating into the tumor interior, the C6 tumor-bearing nude mice intravenously received DiI-labeled LNC, CO-LNC, d-rHDL and s-rHDL at the dose of DMPC 20 mg/kg. Three h after-injection, the mice were anesthetized, and heart perfused with saline and 4% paraformaldehyde. The brains were then collected, fixed in 4% paraformaldehyde and dehydrated in 10%, 30% sucrose solution. Afterward, the brains were imbedded in OCT (Sakura, Torrance, CA, USA), frozen at -80 °C and sectioned at 14 mm. Finally, the slides were subjected to confocal microscopy analysis (LSM710, Leica, Germany) after staining with DAPI for 10 min and rinsing with PBS. Each experimental group consisted of three animals and at least five sections per tumor tissue were analyzed.

3.8. Statistical analysis

All the data were presented as mean ± standard deviation (s.d.). Student's *t*-test was used for two-group comparison. Statistical significance was defined as $p<0.05$.
Acknowledgements: This study was supported by National Key Basic Research Program (2013CB932502), National Natural Science Foundation of China (No. 81373351, 81573382), grants from Shanghai Science and Technology Committee (15540723700, 13NM1400500), Shanghai Talent Development Fund (201459) and Funding from Shanghai Jiao Tong University (YG2014MS75).

Conflicts of interest: None declared.

References

Cabral H, Matsumoto Y, Mizuno K, Chen Q, Murakami M, Kimura M, Terada Y, Kano MR, Miyazono K, Uesaka M, Nishiyama N, Kataoka K (2011) Accumulation of sub-100 nm polymeric micelles in poorly permeable tumours depends on size. Nat Nanotechnol 6: 815-823.

Chauhan VP, Stylianopoulos T, Boucher Y, Jain RK (2011) Delivery of molecular and nanoscale medicine to tumors: transport barriers and strategies. Annu Rev Chem Biomol Eng 2: 281-298.

Cho KH (2009) Biomedicinal implications of high-density lipoprotein: its composition, structure, functions, and clinical applications. BMB Rep 42: 393-400.

Croy JE, Brandon T, Komives EA (2004) Two apolipoprotein E mimetic peptides, ApoE (130-149) and ApoE (141-155) 2, bind to LRP1. Biochemistry 43: 7328-7335.

Das UN (2011) Essential fatty acids and their metabolites as modulators of stem cell biology with reference to inflammation, cancer, and metastasis. Cancer Metastasis Rev 30: 311-324.

Diop-Frimpong B, Chauhan VP, Krane S, Boucher Y, Jain RK (2011) Losartan inhibits collagen I synthesis and improves the distribution and efficacy of nanotherapeutics in tumors. Proc Natl Acad Sci U S A 108: 2909-2914.

Ernsting MJ, Murakami M, Roy A, Li SD (2013) Factors controlling the pharmacokinetics, biodistribution and intratumoral penetration of nanoparticles. J Control Release 172: 782-794.

Fang J, Nakamura H, Maeda H (2011) The EPR effect: Unique features of tumor blood vessels for drug delivery, factors involved, and limitations and augmentation of the effect. Adv Drug Deliv Rev 63: 136-151.

Foster DA (2013) Phosphatidic acid and lipid-sensing by mTOR. Trends Endocrinol Metab 24: 272-278.

Gessner A, Lieske A, Paulke B, Muller R (2002) Influence of surface charge density on protein adsorption on polymeric nanoparticles: analysis by two-dimensional electrophoresis. Eur J Pharm Biopharm 54: 165-170.

Grossman SA, Ye X, Piantadosi S, Desideri S, Nabors LB, Rosenfeld M, Fisher J (2010) Survival of patients with newly diagnosed glioblastoma treated with radiation and temozolomide in research studies in the United States. Clin Cancer Res 16: 2443-2449.

Hendricks BK, Cohen-Gadol AA, Miller JC (2015) Novel delivery methods bypassing the blood-brain and blood-tumor barriers. Neurosurg Focus 38: E10.

Hirschhaeuser F, Menne H, Dittfeld C, West J, Mueller-Klieser W, Kunz-Schughart LA (2010) Multicellular tumor spheroids: an underestimated tool is catching up again. J Biotechnol 148: 3-15.

Huang M, Hu M, Song Q, Song H, Huang J, Gu X, Wang X, Chen J, Kang T, Feng X, Jiang D, Zheng G, Chen H, Gao X (2015) GM1-Modified Lipoprotein-like Nanoparticle: Multifunctional Nanoplatform for the Combination Therapy of Alzheimer's Disease. ACS Nano 9: 10801-10816.

Jain RK, Duda DG, Clark JW, Loeffler JS (2006) Lessons from phase III clinical trials on anti-VEGF therapy for cancer. Nat Clin Pract Oncol 3: 24-40.

Kuai R, Li D, Chen YE, Moon JJ, Schwendeman A (2016) High-density lipoproteins: nature's multifunctional nanoparticles. ACS Nano 10: 3015-3041.

Lee H, Fonge H, Hoang B, Reilly RM, Allen C (2010) The effects of particle size and molecular targeting on the intratumoral and subcellular distribution of polymeric nanoparticles. Mol Pharm 7: 1195-1208.

Levchenko TS, Rammohan R, Lukyanov AN, Whiteman KR, Torchilin VP (2002) Liposome clearance in mice: the effect of a separate and combined presence of surface charge and polymer coating. Int J Pharm 240: 95-102.

Li SD, Huang L (2008) Pharmacokinetics and biodistribution of nanoparticles. Mol Pharm 5: 496-504.

Li YC, Park MJ, Ye SK, Kim CW, Kim YN (2006) Elevated levels of cholesterol-rich lipid rafts in cancer cells are correlated with apoptosis sensitivity induced by cholesterol-depleting agents. Am J Pathol 168: 1107-1118.

Liang HQ, Rye KA, Barter PJ (1996) Remodelling of reconstituted high density lipoproteins by lecithin: cholesterol acyltransferase. J Lipid Res 37: 1962-1970.

Lin Q, Chen J, Jin H, Ng KK, Yang M, Cao W, Ding L, Zhang Z, Zheng G (2012) Efficient systemic delivery of siRNA by using high-density lipoprotein-mimicking peptide lipid nanoparticles. Nanomedicine (Lond) 7: 1813-1825.

McConathy WJ, Nair MP, Paranjape S, Mooberry L, Lacko AG (2008) Evaluation of synthetic/reconstituted high-density lipoproteins as delivery vehicles for paclitaxel. Anticancer Drugs 19: 183-188.

Mooberry LK, Nair M, Paranjape S, McConathy WJ, Lacko AG (2010) Receptor mediated uptake of paclitaxel from a synthetic high density lipoprotein nanocarrier. J Drug Target 18: 53-58.

Ng KK, Lovell JF, Zheng G (2011) Lipoprotein-inspired nanoparticles for cancer theranostics. Acc Chem Res 44: 1105-1113.

Oberoi RK, Parrish KE, Sio TT, Mittapalli RK, Elmquist WF, Sarkaria JN (2016) Strategies to improve delivery of anticancer drugs across the blood-brain barrier to treat glioblastoma. Neuro Oncol 18: 27-36.

Prevost M, Raussens V (2004) Apolipoprotein E-low density lipoprotein receptor binding: study of protein-protein interaction in rationally selected docked complexes. Proteins 55: 874-884.

Rader DJ (2006) Molecular regulation of HDL metabolism and function: implications for novel therapies. J Clin Invest 116: 3090-3100.

Salloum D, Mukhopadhyay S, Tung K, Polonetskaya A, Foster DA (2014) Mutant ras elevates dependence on serum lipids and creates a synthetic lethality for rapamycin. Mol Cancer Ther 13: 733-741.

Siegel R, Naishadham D, Jemal A (2013) Cancer statistics, 2013. CA Cancer J Clin 63: 11-30.

Song Q, Huang M, Yao L, Wang X, Gu X, Chen J, Chen J, Huang J, Hu Q, Kang T, Rong Z, Qi H, Zheng G, Chen H, Gao X (2014) Lipoprotein-based nanoparticles rescue the memory loss of mice with Alzheimer's disease by accelerating the clearance of amyloid-beta. ACS Nano 8: 2345-2359.

Tong RT, Boucher Y, Kozin SV, Winkler F, Hicklin DJ, Jain RK (2004) Vascular normalization by vascular endothelial growth factor receptor 2 blockade induces a pressure gradient across the vasculature and improves drug penetration in tumors. Cancer Res 64: 3731-3736.

Vickers KC, Palmisano BT, Shoucri BM, Shamburek RD, Remaley AT (2011) MicroRNAs are transported in plasma and delivered to recipient cells by high-density lipoproteins. Nature Cell Biology 13: 423-433.

Wang J, Jia J, Liu J, He H, Zhang W, Li Z (2013) Tumor targeting effects of a novel modified paclitaxel-loaded discoidal mimic high density lipoproteins. Drug Deliv 20: 356-363.

Wang Y, Wang D, Fu Q, Liu D, Ma Y, Racette K, He Z, Liu F (2014) Shape-controlled paclitaxel nanoparticles with multiple morphologies: rod-shaped, worm-like, spherical, and fingerprint-like. Mol Pharm 11: 3766-3771.

Zhang B, Sun X, Mei H, Wang Y, Liao Z, Chen J, Zhang Q, Hu Y, Pang Z, Jiang X (2013) LDLR-mediated peptide-22-conjugated nanoparticles for dual-targeting therapy of brain glioma. Biomaterials 34: 9171-9182.

Zhang W, He H, Liu J, Wang J, Zhang S, Zhang S, Wu Z (2013) Pharmacokinetics and atherosclerotic lesions targeting effects of tanshinone IIA discoidal and spherical biomimetic high density lipoproteins. Biomaterials 34: 306-319.

Zhang WL, Xiao Y, Liu JP, Wu ZM, Gu X, Xu YM, Lu H (2011) Structure and remodeling behavior of drug-loaded high density lipoproteins and their atherosclerotic plaque targeting mechanism in foam cell model. Int J Pharm 419: 314-321.